

Stable long-term evolution in numerical relativity

Sebastian Garcia-Saenz^{a,*}, Guangzhou Guo^{a,†}, Peng Wang^{b,‡}, Xinmiao Wang^{a,§}

^a*Department of Physics, Southern University of Science and Technology,
Shenzhen 518055, China*

^b*Center for Theoretical Physics, College of Physics, Sichuan University,
Chengdu 610064, China*

We report on the potential occurrence of a numerical instability in the long-time simulation of black holes using the Baumgarte-Shapiro-Shibata-Nakamura formulation of numerical relativity, even in the simple set-up of a Schwarzschild black hole. Through extensive numerical experiments, we identify that this “late-time instability” arises from accumulated violations of the momentum constraint. To address this issue, we propose two modified versions of the so-called conformal covariant Z4 scheme, designed to propagate momentum constraint violations without damping. Our results demonstrate that these alternative formulations, which we refer to as CCZ4’ and CCZ3, effectively resolve the late-time numerical instability not only in Schwarzschild spacetimes but also in black hole spacetimes with matter fields. Notably, by preventing damping of the momentum constraint violation, the Hamiltonian constraint damping can be significantly increased, which plays a crucial role in stabilizing long-term evolution in our proposed schemes.

* sgarciasaenz@sustech.edu.cn

† guogz@sustech.edu.cn

‡ pengw@scu.edu.cn

§ 12132943@mail.sustech.edu.cn

CONTENTS

I. Introduction	2
II. Numerical schemes for evolving the Einstein equations	4
III. Stable evolution of black hole spacetimes	8
A. Late-time numerical instability	9
B. Modified numerical schemes	10
IV. Applications to non-vacuum black holes	13
A. Numerical evolution of matter fields	14
B. RN black hole	16
C. Spontaneous scalarization	16
V. Conclusions	18
Acknowledgments	19
References	20

I. INTRODUCTION

Recent observational breakthroughs in black hole physics [1–3] underscore the need for stable, long-time numerical relativity simulations to study black hole evolution, particularly in systems affected by weak instabilities characterized by very long time scales. Investigating the evolution of such systems through numerical relativity cannot only provide gravitational wave templates for experiments, but also help explore and understand their theoretical properties [4–7].

A remarkable example of such weak instabilities is the superradiant extraction of mass from a spinning black hole by a massive probe scalar field [8, 9]. In this process, the mass of the scalar field serves as a reflective outer boundary, enabling continuous mass extraction from the black hole, leading to the formation of a scalar cloud encircling it [10]. However, the growth rate of such superradiant instabilities is extremely slow, posing significant numerical challenges for studying the long-term evolution of this phenomenon [11, 12]. To evade this issue, research on the non-linear evolution of these set-ups has shifted to scenarios involving a charged scalar field around a charged black hole or a massive vector field around a spinning black hole, where the

instability rates are significantly faster [13, 14]. Despite this advantage, the studies still require robust numerical techniques capable of simulating long-term evolution. It has been shown, for instance, that a saturated cloud of massive vectors can radiate slowly through gravitational wave emission over time-scales extending to about 10^5 in units of the initial black hole mass, as the hole spins down and exits the superradiant regime [14]. In addition to superradiance, weak non-linear instabilities have also been reported in spacetimes featuring a stable light ring [15, 16]. Numerical studies suggest that exotic compact objects may experience light-ring instabilities after long-term evolution [16]. Conversely, simulations indicate that black holes with multiple photon spheres appear free of such instabilities, even after extended evolution [7], although again diagnosing this outcome is only possible by means of long-term simulations.

One of the most remarkable developments in numerical relativity has been the Baumgarte-Shapiro-Shibata-Nakamura (BSSN) formulation [17, 18], which is widely used for its accuracy and stability in simulating black hole evolution, particularly for modeling binary mergers and computing gravitational waves [4–6]. The BSSN formalism is based on the construction of a conformal connection as an evolution variable in a specific coordinate system, in order to ensure strong hyperbolicity through the application of the momentum constraint equation. Subsequently, the BSSN formulation has been generalized to a covariant form by introducing a reference metric [19–22]. This generalized scheme allows for the definition of a covariant and conformal connection, facilitating black hole evolution in coordinate patches that optimize computational efficiency.

On the other hand, the BSSN formulation does not propagate Hamiltonian constraint violations. To address this limitation, the so-called conformal covariant Z4 system (CCZ4), and the related Z4c, have been proposed, in which constraint violations are promoted to dynamical variables [23–25]. The CCZ4 formulation effectively converts the violations of the Hamiltonian and momentum constraints into wave propagation equations. In contrast, the Z4c formulation focuses solely on propagating the Hamiltonian constraint violation, preserving a structure closer to the BSSN formulation [25, 26]. Similarly to the generalized BSSN formulation, the CCZ4 formulation has also been extended to a fully covariant form by introducing an additional reference metric [27–29]. While the CCZ4 formulation has demonstrated higher accuracy in simulating binary neutron stars compared to the BSSN formulation, it suffers from non-linear numerical instabilities when applied to black hole spacetimes. As shown in previous studies [27, 30], these instabilities can be alleviated by adequately introducing damping for the constraint violations. However, a key observation is that the damping effect must not be excessively strong to avoid the emergence of further numerical instabilities.

The purpose of this paper is to develop a numerical scheme that ensures stable, long-term evolution and can be applied to studying the ultimate fate of systems afflicted by the aforementioned weak instabilities. The rest of the paper is organized as follows. In Section II, we review several numerical schemes for solving the time evolution of the Einstein equations, and introduce two new proposals specifically tailored for long-term numerical stability, which we dub CCZ4' and CCZ3 schemes, which are characterized by the propagation of the violations of the momentum constraints without damping. In Section III, we demonstrate that the CCZ4' and CCZ3 formulations enable stable evolution of a Schwarzschild black hole over time-scales up to 10^5 in units of the black hole's mass. Section IV explores the application of these schemes to the fully non-linear evolution of matter fields in black hole spacetimes, showing that the CCZ3 formulation appears to offer the highest degree of stability and accuracy for studying systems with weak instabilities. We close with a summary of our findings and conclusions in Section V. Throughout this paper, we adopt units with $G = c = 4\pi\epsilon_0 = 1$.

II. NUMERICAL SCHEMES FOR EVOLVING THE EINSTEIN EQUATIONS

To numerically evolve the metric variables, we adopt the fully covariant and conformal formulation of the Einstein field equations in the context of the damped Z4 (CCZ4) system [23, 30]. The CCZ4 scheme is specifically designed for numerical relativity simulations, where the Einstein equations are reformulated to improve the numerical stability and accuracy. In this system, the Einstein equation is extended to

$${}^{(4)}R_{\mu\nu} + 2\nabla_{(\mu}{}^{(4)}Z_{\nu)} - \kappa_1 \left[2n_{(\mu}{}^{(4)}Z_{\nu)} - (1 + \kappa_2) g_{\mu\nu} n^\rho{}^{(4)}Z_\rho \right] = 8\pi \left(T_{\mu\nu} - \frac{1}{2} g_{\mu\nu} T \right), \quad (1)$$

where ${}^{(4)}R_{\mu\nu}$ is the four-dimensional Ricci tensor associated with the metric $g_{\mu\nu}$, ∇_μ is the covariant derivative, and $T_{\mu\nu}$ is the stress-energy tensor (with $T \equiv T^\mu{}_\mu$). Here, the four-vector ${}^{(4)}Z_\mu$ quantifies deviations from the Einstein equation, particularly important for keeping track of constraint violations during numerical evolution. When ${}^{(4)}Z_\mu = 0$, the system reduces to the standard Einstein equation. The constants κ_1 and κ_2 are damping parameters introduced to control the magnitude of ${}^{(4)}Z_\mu$ in numerical simulations. The normal vector to the three-dimensional spatial hypersurface Σ is denoted by n_μ , pointing along the time evolution of the foliation Σ in the future direction.

In the 3+1 decomposition of spacetime, the line element is expressed in terms of ADM variables

as

$$ds^2 = -\alpha^2 dt^2 + \gamma_{ij} (dx^i + \beta^i dt) (dx^j + \beta^j dt), \quad (2)$$

where α is the lapse function, β^i is the shift vector, and γ_{ij} is the induced physical metric on Σ . The normal vector is given by $n_\mu = (-\alpha, 0, 0, 0)$, or $n^\mu = (1/\alpha, -\beta^i/\alpha)$.

Using Bianchi identities, taking the divergence of the modified Einstein equation (1) yields a propagation equation for ${}^{(4)}Z_\mu$,

$$\square {}^{(4)}Z_\mu = -R_{\mu\nu} {}^{(4)}Z^\nu - \kappa_1 \nabla^\nu \left(n_\mu {}^{(4)}Z_\nu + n_\nu {}^{(4)}Z_\mu + \kappa_2 g_{\mu\nu} n_\sigma {}^{(4)}Z^\sigma \right), \quad (3)$$

which governs the evolution of constraint violations ${}^{(4)}Z_\mu$. In weakly curved spacetimes, this approximates a standard damped wave equation. Here, κ_1 and κ_2 serve as damping factors aimed at suppressing the amount of violation of the constraints. In the 3+1 decomposition, ${}^{(4)}Z_\mu$ is split into components along the normal vector n^μ and directions tangential to the spatial hypersurface Σ ,

$$\Theta = -n_\mu {}^{(4)}Z^\mu, \quad Z_i = \gamma_i^\mu {}^{(4)}Z_\mu, \quad (4)$$

where the projection operator is $\gamma_i^\nu = \delta_i^\nu + n_i n^\nu$. Similarly, the stress-energy tensor $T_{\mu\nu}$ is decomposed as

$$\rho = n^\mu n^\nu T_{\mu\nu}, \quad S_i = -\gamma_i^\mu n^\nu T_{\mu\nu}, \quad S_{ij} = \gamma_i^\mu \gamma_j^\nu T_{\mu\nu}. \quad (5)$$

From Eq. (3), the evolution equations for Θ and Z_i in terms of the ADM variables read

$$\partial_\perp \Theta = \frac{\alpha}{2} (R + K^2 - K_{ij} K^{ij} - 16\pi\rho) - \alpha\Theta K + \alpha D_i Z^i - Z^i \partial_i \alpha - \alpha\kappa_1 (2 + \kappa_2) \Theta, \quad (6)$$

$$\partial_\perp Z_i = \alpha \left(D_j K_i^j - D_i K - 8\pi S_i \right) + \alpha \partial_i \Theta - 2\alpha K_i^j Z_j - \Theta \partial_i \alpha - \kappa_1 \alpha Z_i, \quad (7)$$

where $\partial_\perp \equiv \partial_t - \mathcal{L}_\beta$ and $K_{ij} \equiv -\mathcal{L}_n \gamma_{ij}/2$ is the extrinsic curvature of the hypersurface Σ . In the absence of constraint violations (i.e., ${}^{(4)}Z_\mu = 0$), the ADM Hamiltonian and momentum constraints of general relativity are recovered as

$$H = \frac{1}{2} (R + K^2 - K_{ij} K^{ij}) - 8\pi\rho = 0, \quad (8)$$

$$M_i = D_j K_i^j - D_i K - 8\pi S_i = 0. \quad (9)$$

Comparing Eqs. (8) and (9) with Eqs. (6) and (7), it is evident that Θ characterizes the Hamiltonian constraint violation while Z_i measures the momentum constraint violation. Therefore the evolution

equations for Θ and Z_i (Eqs. (6) and (7)) describe the propagation of constraint violations during numerical simulations.

In this paper, we focus on the fully covariant and conformal formulations of numerical relativity. To achieve a conformal formulation, the spatial metric γ_{ij} is decomposed as

$$\gamma_{ij} = e^{4\phi} \bar{\gamma}_{ij}, \quad (10)$$

where $e^{4\phi}$ is the conformal factor. In addition, we impose Brown's Lagrangian condition $\partial_t \bar{\gamma} = 0$, where $\bar{\gamma}$ represents the determinant of the conformal metric $\bar{\gamma}_{ij}$ [19]. In this conformal formalism, the extrinsic curvature is rescaled as

$$\bar{A}_{ij} = e^{-4\phi} \left(K_{ij} - \frac{1}{3} \gamma_{ij} K \right). \quad (11)$$

To implement a fully covariant formulation, a reference metric $\hat{\gamma}_{ij}$ is introduced as a fixed background that remains static throughout the simulation. Using this reference metric, a covariant connection is defined by the difference

$$\Delta \Gamma_{jk}^i \equiv \bar{\Gamma}_{jk}^i - \hat{\Gamma}_{jk}^i, \quad (12)$$

where $\bar{\Gamma}_{jk}^i$ is the connection associated with the conformal metric $\bar{\gamma}_{ij}$ and $\hat{\Gamma}_{jk}^i$ is the connection associated with the reference metric $\hat{\gamma}_{ij}$.

Collecting all equations in this formulation we arrive at the following CCZ4 system [20, 27]:

$$\partial_{\perp} \bar{\gamma}_{ij} = \frac{2}{3} \bar{\gamma}_{ij} \left(\alpha \bar{A}_k^k - \bar{D}_k \beta^k \right) - 2\alpha \bar{A}_{ij}, \quad (13)$$

$$\begin{aligned} \partial_{\perp} \bar{A}_{ij} = & e^{-4\phi} \left[-2\alpha \bar{D}_i \bar{D}_j \phi + 4\alpha \bar{D}_i \phi \bar{D}_j \phi + 4\bar{D}_{(i} \alpha \bar{D}_{j)} \phi - \bar{D}_i \bar{D}_j \alpha + \alpha \left(\bar{R}_{ij} + 2D_{(i} Z_{j)} - 8\pi S_{ij} \right) \right]^{\text{TF}} \\ & - \frac{2}{3} \bar{A}_{ij} \bar{D}_k \beta^k - 2\alpha \bar{A}_{ik} \bar{A}_j^k + \alpha \bar{A}_{ij} (K - 2\Theta), \end{aligned} \quad (14)$$

$$\begin{aligned} \partial_{\perp} K = & e^{-4\phi} \left[\alpha \left(\bar{R} - 8\bar{D}^i \phi \bar{D}_i \phi - 8\bar{D}^2 \phi \right) - \left(2\bar{D}^i \alpha \bar{D}_i \phi + \bar{D}^2 \alpha \right) \right] + \alpha \left(K^2 - 2\Theta K \right) \\ & + 2\alpha D_i Z^i - 3\alpha \kappa_1 (1 + \kappa_2) \Theta + 4\pi \alpha (S - 3\rho), \end{aligned} \quad (15)$$

$$\partial_{\perp} \phi = \frac{1}{6} \bar{D}_k \beta^k - \frac{1}{6} \alpha K, \quad (16)$$

$$\partial_{\perp} \Theta = \frac{1}{2} \alpha \left[e^{-4\phi} \left(\bar{R} - 8\bar{D}^i \phi \bar{D}_i \phi - 8\bar{D}^2 \phi \right) - \bar{A}_{ij} \bar{A}^{ij} + \frac{2}{3} K^2 - 2\Theta K + 2D_i Z^i \right], \quad (17)$$

$$\begin{aligned} \partial_{\perp} \tilde{\Lambda}^i = & \bar{\gamma}^{jk} \hat{D}_j \hat{D}_k \beta^i + \frac{2}{3} \tilde{\Lambda}^i \bar{D}_j \beta^j + \frac{1}{3} \bar{D}^i \bar{D}_j \beta^j - 2\bar{A}^{ij} (\partial_j \alpha - 6\alpha \partial_j \phi) + 2\alpha \bar{A}^{jk} \Delta \Gamma_{jk}^i \\ & - \frac{4}{3} \alpha \bar{\gamma}^{ij} \partial_j K + 2\bar{\gamma}^{ij} \left(\alpha \partial_j \Theta - \Theta \partial_j \alpha - \frac{2}{3} \alpha K Z_j \right) - 2\alpha \kappa_1 \bar{\gamma}^{ij} Z_j - 16\pi \alpha \bar{\gamma}^{ij} S_j, \end{aligned} \quad (18)$$

where 'TF' denotes the trace-free part of the corresponding tensor. Here, \hat{D}_i , \bar{D}_i and D_i represent the covariant derivatives with respect to the reference metric $\hat{\gamma}_{ij}$, the conformal metric $\bar{\gamma}_{ij}$, and the

ADM metric γ_{ij} , respectively. In Eq. (18), the dynamical variable $\tilde{\Lambda}^i$ is defined as

$$\tilde{\Lambda}^i \equiv \bar{\Lambda}^i + 2\bar{\gamma}^{ij}Z_j, \quad (19)$$

with $\bar{\Lambda}^i \equiv \bar{\gamma}^{jk}\Delta\Gamma_{jk}^i$. We remark that the evolution equation for $\bar{\Lambda}^i$ can also be derived from the momentum constraint equation, indicating it is not independent of Eq. (7). In the CCZ4 formulation, Eq. (18) governing $\tilde{\Lambda}^i$ serves two purposes: it functions like $\bar{\Lambda}^i$ in the BSSN formulation for constructing a strongly hyperbolic system and also propagates momentum constraint violations as in Eq. (7).

Regarding the fixing of gauge, we employ the 1 + log slicing condition for the lapse field α and the Γ -driving condition for the shift vector field β^i [20, 31–33],

$$\partial_{\perp}\alpha = -2\alpha(K - 2\Theta), \quad (20)$$

$$\partial_{\perp}\beta^i = C^i,$$

$$\partial_{\perp}C^i = \frac{3}{4}\partial_{\perp}\tilde{\Lambda}^i - \eta C^i, \quad (21)$$

where C^i is an auxiliary field and η is another damping parameter, and for simplicity we choose $\eta = 1$ throughout this paper.

In accordance with our aim of comparing different numerical schemes, we introduce the following schemes as alternatives to the CCZ4 formulation outlined above:

BSSN: This formulation is composed of Eqs. (13), (14), (16), and together with

$$\partial_{\perp}K = \frac{1}{3}\alpha K^2 + \alpha\bar{A}_{ij}\bar{A}^{ij} - e^{-4\phi}(2\bar{D}^i\alpha\bar{D}_i\phi + \bar{D}^2\alpha), \quad (22)$$

$$\begin{aligned} \partial_{\perp}\bar{\Lambda}^i &= \bar{\gamma}^{jk}\hat{D}_j\hat{D}_k\beta^i + \frac{2}{3}\bar{\Lambda}^i\bar{D}_j\beta^j + \frac{1}{3}\bar{D}^i\bar{D}_j\beta^j - 2\bar{A}^{ij}(\partial_j\alpha - 6\alpha\partial_j\phi) \\ &\quad + 2\alpha\bar{A}^{jk}\Delta\Gamma_{jk}^i - \frac{4}{3}\alpha\bar{\gamma}^{ij}\partial_jK - 16\pi\alpha\bar{\gamma}^{ij}S_j. \end{aligned} \quad (23)$$

In this formulation, Θ and Z_i are set to zero in all equations.

CCZ4': This formulation follows the equations of the CCZ4 systems as defined in Eqs. (13), (14), (15), (16), (17) and (18). However, the damping factor κ_1 is replaced by κ_{Θ} in Eq. (15) and by κ_{Γ} in Eq. (18). In other words, we allow for different damping factors in these two equations.

CCZ0: This formulation consists of the same equations as the CCZ4 system: (13), (14), (15), (16), (17) and (18), except that $Z_i = 0$ is set in all equations.

CCZ3: This formulation uses the evolution equations (13), (14), (15), (16) and (18). In this formulation, $\Theta = 0$ is set in all equations.

The CCZ4' and CCZ3 formulations correspond to our new proposals, which we will show to be effective for the purpose of long-term black hole evolution and the related question of numerical stability. On the other hand, the BSSN and CCZ0 will instead be used for the purpose of comparison and for explaining the advantages of our formulations.

III. STABLE EVOLUTION OF BLACK HOLE SPACETIMES

In this Section, we study the application of the numerical schemes discussed in the previous Section to long-term simulations of black hole evolution. Numerical experiments with a Schwarzschild black hole reveal that the standard numerical scheme, specifically the BSSN formulation, exhibits numerical instabilities during long-time simulations. We trace the source of these instabilities to violations of the momentum constraint. We then show that our modified numerical schemes, namely CCZ4' and CCZ3, succeed in addressing this issue by ensuring long-term stability in black hole simulations.

We integrate the numerical framework reviewed in Section II into the *BlackHoles@Home* platform [34]. For practical implementation, we employ a reference metric given by

$$\hat{dl}^2 = dr^2 + r^2 d\Omega = (dr/dR)^2 dR^2 + r(R)^2 d\Omega, \quad (24)$$

in spherical-like coordinates (R, θ, φ) . Here, the radial coordinate r is scaled to a dimensionless quantity R by

$$r = r_{max} \left(RR_0 + \frac{e^{R/a} - e^{-R/a}}{e^{1/a} - e^{-1/a}} \right), \quad (25)$$

where r_{max} denotes the outer boundary in the numerical simulation, and R_0 and a are scaling factors linking r and R . This transformation maps the radial range $[0, r_{max}(R_0 + 1)]$ onto $[0, 1]$, and note that $r_{max}(R_0 + 1) \approx r_{max}$ since R_0 is chosen to be very small. Notice that we restrict our attention to spherically symmetric systems in this paper. Radial discretization is achieved using a uniform grid in the rescaled coordinate R , with a grid size of N_R cells. To stabilize the simulations and mitigate high-frequency numerical noise, we apply the Kreiss-Oliger (KO) dissipation technique to all evolved variables. Additionally, we consider the Courant-Friedrichs-Lewy (CFL) condition (see e.g. [35]), defined by the factor

$$\text{CFL} = \frac{\Delta t}{\Delta r_{min}}, \quad (26)$$

where Δr_{min} is the smallest spatial step in the grid. To maintain numerical stability, the CFL factor must not exceed one, ensuring that information does not propagate more than one grid cell during a single time step. We use fourth-order finite differential on the spatial direction, and forth-order Runge-Kutta for the time integration.

The benchmark parameters used in our simulations are as follows:

$$r_{max} = 60000M, R_0 = 0.00012, a = 0.07, N_R = 300, \epsilon_{KO} = 0.2, \text{CFL} = 1.0, \quad (27)$$

where ϵ_{KO} specifies the strength of the KO dissipation. Here and in what follows, M is the initial mass of the black hole. Unless otherwise stated, these parameters (27) are used as the default settings for numerical evolution in this study. In the following, we simulate the area of the apparent horizon A_h for the purpose of examining the numerical stability.

A. Late-time numerical instability

For the numerical evolution of an isolated black hole, we employ pre-collapsed initial data representing a Schwarzschild black hole. This configuration transitions from a wormhole slice to a trumpet slice using the moving puncture method [4, 6, 36]. The initial data for the spacetime is given by

$$e^\phi = 1 + \frac{M}{2r}, \quad (28)$$

with pre-collapsed lapse $\alpha = e^{-2\phi}$ and vanishing shift $\beta^i = 0$.

In Fig. 1, we present the results of our simulations of the evolution of a Schwarzschild black hole within the BSSN formulation, using various numerical parameter settings. The upper-left panel compares different scaling parameters, where $r_{max} = 500M$, $R_0 = 0.0015$, $a = 0.15$ (orange line); $r_{max} = 1000M$, $R_0 = 0.001$, $a = 0.12$ (green); and $r_{max} = 60000M$, $R_0 = 0.0012$, $a = 0.07$ (blue). For smaller values of r_{max} , noticeable numerical perturbations emerge due to noise from the outer boundary during the simulation. The upper-right panel varies grid numbers: $N_R = 200$ (orange), $N_R = 300$ (blue) and $N_R = 400$ (green). Simulations with fewer grid points ($N_R = 200$) exhibit more pronounced numerical errors compared to higher-resolution set-ups ($N_R = 300$ or 400). The lower-left panel examines dissipation schemes with $\epsilon_{KO} = 0.1$ (orange), $\epsilon_{KO} = 0.2$ (green) and $\epsilon_{CAKO} = 0.2$ (blue). Here, $\epsilon_{CAKO} = e^{-2\phi}\epsilon_{KO}$ is the curvature-adjusted KO dissipation strength, which was proposed to reduce numerical noise near the puncture by an additional dissipation term [37]. Lastly, the dependence on the CFL factor is tested in the lower-right panel: $\text{CFL} = 0.3$

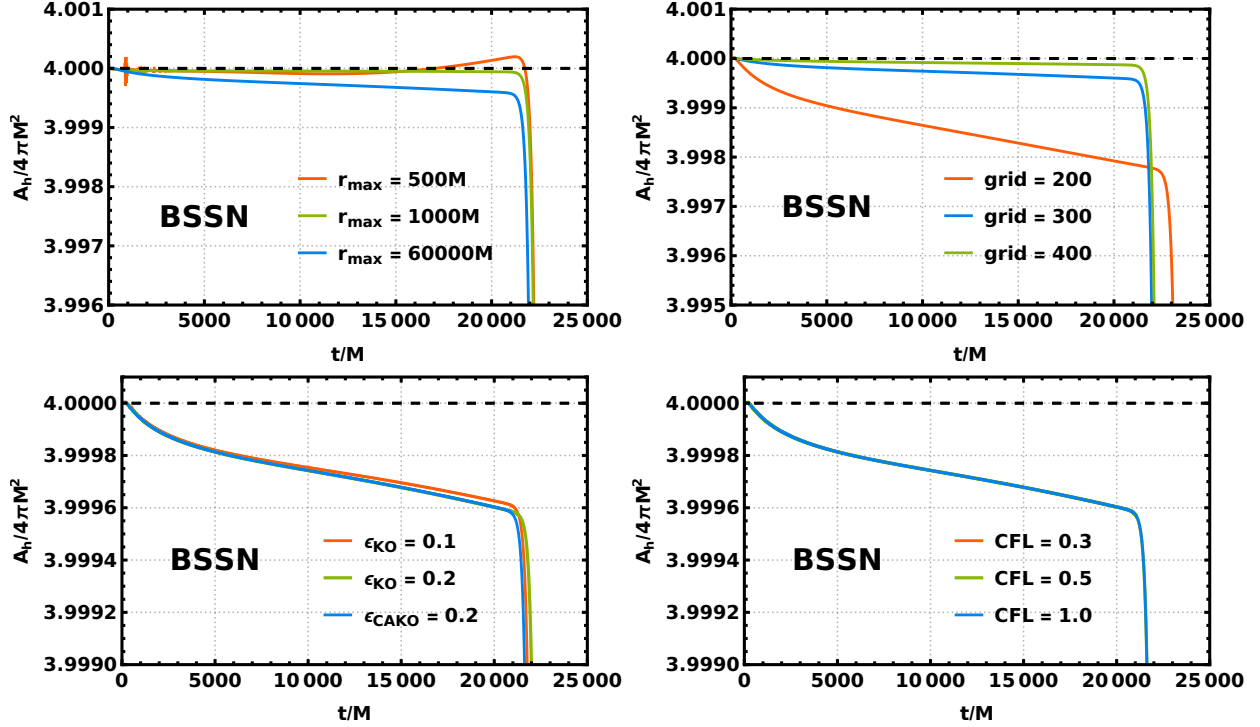


FIG. 1. Schwarzschild black hole evolution, as measured by the area of the apparent horizon, A_h , under various parameter settings. These include different scaling parameters (upper-left panel), varying grid numbers (upper-right), applying different dissipation schemes (lower-left), and different CFL factors (lower-right). See the main text for further details. The results demonstrate that the numerical instability persists at late times irrespective of parameter adjustments.

(orange), CFL = 0.5 (green), CFL = 1.0 (blue); the variation in this case is essentially negligible, as seen in the graph where all three curves overlap.

The clear lesson revealed by the simulations is the presence of a late-time numerical instability that persists for a broad range of parameter adjustments. These findings suggest that this “late-time instability” is an essential aspect of the numerical formulation rather than the parameter settings.

B. Modified numerical schemes

In the BSSN formulation, constraint violations are not part of the evolution equations of the system. Numerical errors, which are unavoidable in practical computations, can arise from truncation in finite differencing during spatial discretization, inaccuracies in time integration using the Runge-Kutta algorithm, or precision loss after numerous iterations. Without appropriate miti-

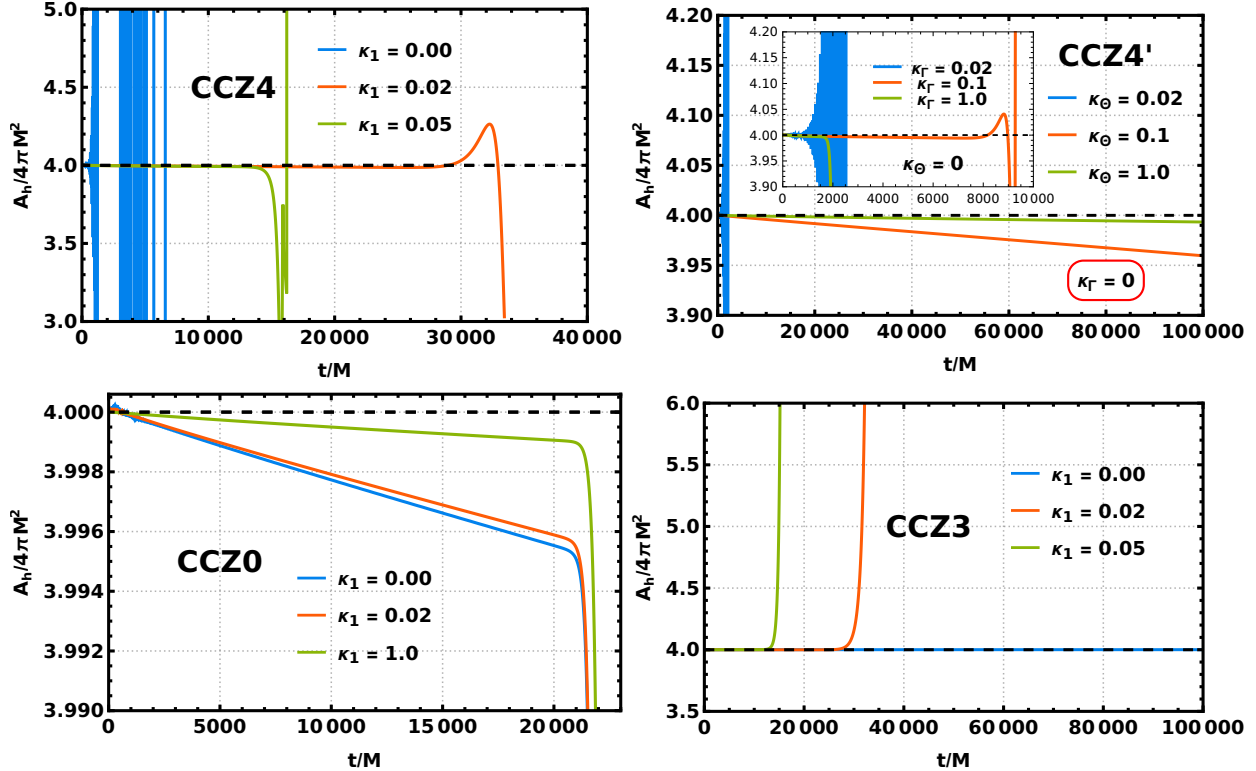


FIG. 2. Numerical evolution of a Schwarzschild black hole, as measured by the area of the apparent horizon, A_h , under different numerical schemes. *Upper-left panel:* The CCZ4 formulation demonstrates that κ_1 impacts numerical stability, with nonlinear instabilities suppressed by moderate damping but exacerbated by excessive damping. *Upper-right:* The modified CCZ4' formulation considers two different damping parameters in place of κ_1 , i.e. κ_Θ and κ_Γ , with the results showing that suppressing momentum constraint violations ($\kappa_\Gamma = 0$) stabilizes the simulation, while omitting Hamiltonian constraint damping causes instabilities. *Lower-left:* The CCZ0 formulation, which disables momentum constraint propagation ($Z_i = 0$), is seen to exhibit a “late-time instability” similar to the BSSN formulation. *Lower-right:* The CCZ3 formulation, defined by the disabling of the propagation of the Hamiltonian constraint ($\Theta = 0$), effectively removes late-time instabilities in the absence of damping, but is seen to introduce new instabilities when damping terms are applied.

gation, these errors can accumulate, specifically during black hole evolution, causing constraint violations (Θ and Z_i) to grow significantly, potentially leading to numerical instabilities at late times. Thus we anticipate that the “late-time instability” we have identified already in the simple set-up of a Schwarzschild black hole, within the BSSN formulation, may potentially be removed by employing the CCZ4 formulation, or its modified versions proposed here, which are designed to propagate constraint violations.

In Fig. 2, we present the numerical evolution of a Schwarzschild black hole using different

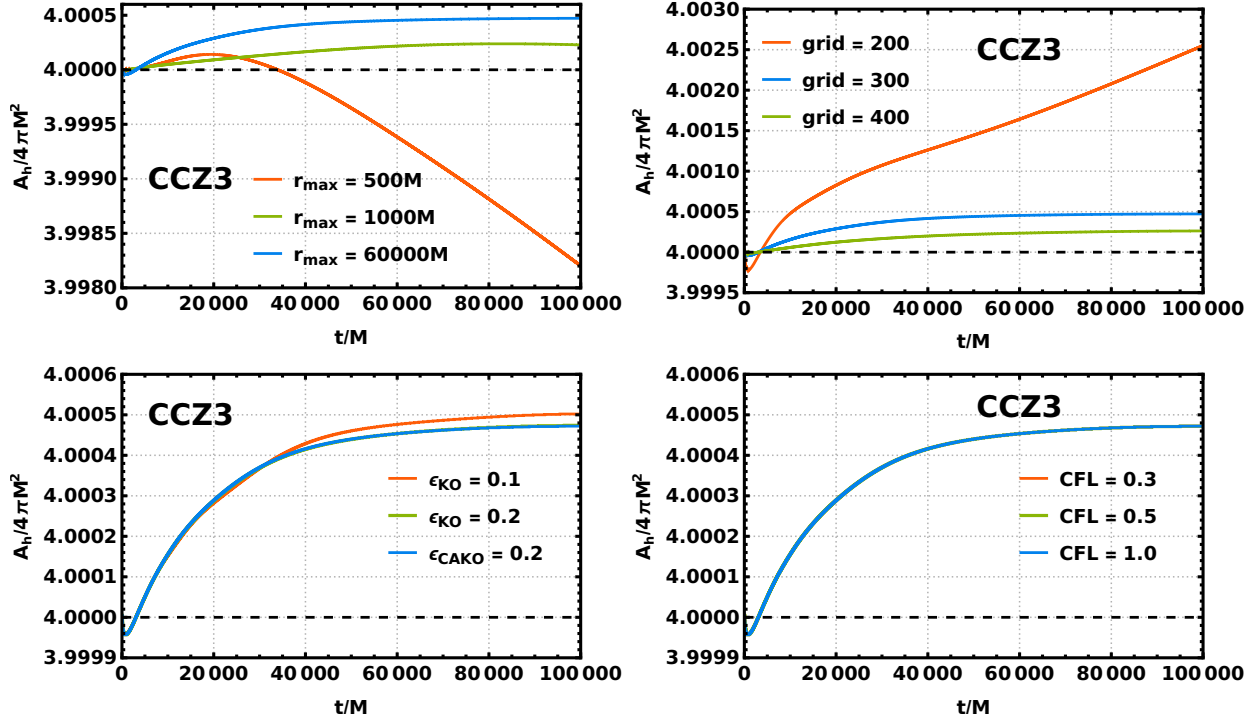


FIG. 3. Numerical evolution of a Schwarzschild black hole, as measured by the area of the apparent horizon, A_h , using the CCZ3 formulation. The “late-time instability” is seen to be absent for all parameter settings used in the previous analysis, cf. Fig. 1, with numerical errors remaining small throughout the simulation.

numerical schemes, where in all cases we have set $\kappa_2 = 0$ (a choice which ensures appropriate damping [38] and is commonly made in the literature). In the upper-left panel, the results indicate that κ_1 has a significant impact on the numerical stability in the CCZ4 formulation. Non-linear effects arising from constraint violations can destabilize the simulation, as shown by the blue curve. As reported in [27, 30], introducing the damping factor κ_1 indeed helps alleviate these instabilities. However, excessively large values of κ_1 can lead to other numerical instabilities, as illustrated by the green line ($\kappa_1 = 0.05$). While the CCZ4 formulation offers slight improvements in long-term stability over the BSSN formulation, it is clear that it does not fully resolve the “late-time instability” issue.

The upper-right panel examines our first modified scheme, what we refer to as CCZ4’ formulation, where κ_1 is replaced by κ_Θ , which damps the Hamiltonian constraint violation Θ , and by κ_Γ , which damps momentum constraint violations Z_i . Without damping of the momentum constraint violation ($\kappa_\Gamma = 0$), the numerical instability is found to be suppressed for sufficiently large values of κ_Θ . On the other hand, as shown in the inset, excluding the damping effect for Hamiltonian constraint violations results in unstable simulations regardless of the choice of κ_Γ . This result sug-

gests that, in the CCZ4' formulation, the absence of damping for momentum constraint violations allows for a large κ_Θ to be effective in removing late-time instabilities.

The lower-left panel presents simulations using the CCZ0 formulation, where momentum constraint propagation is disabled by setting $Z_i = 0$. The numerical behavior closely resembles that of the BSSN formulation in Fig. 1, with the presence of late-time instabilities. This outcome clearly shows that the evolution of the breaking of the momentum constraint is key to the issue of long-term evolution.

Finally, in the lower-right panel, we study the scheme that we refer to as CCZ3, where the Hamiltonian constraint propagation is disabled by setting $\Theta = 0$. The numerical results show that the “late-time instability” can be effectively eliminated when the damping term is absent ($\kappa_1 = 0$). However, introducing a damping term leads to the reappearance of numerical instabilities at late times.

To further investigate the robustness of the CCZ3 formulation, we present in Fig. 3 numerical simulations of a Schwarzschild black hole, employing the same parameter settings as in Fig. 1. The results make it manifest that the “late-time instability” is absent in all cases, with numerical errors remaining under control and within a narrow range of deviation. Together with the outcomes of the above analysis, we can infer that the late-time numerical destabilization observed in the previous Section may be attributed to numerical noise arising from violations of the momentum constraint. It is noteworthy that applying a damping effect to the momentum constraint deviation can induce non-linear numerical instabilities, even with small damping values. The clear conclusion is that the evolution of the momentum constraint violations Z_i , without the introduction of damping terms, is key for achieving robust long-term simulations of black holes.

IV. APPLICATIONS TO NON-VACUUM BLACK HOLES

We study next the application of the numerical schemes discussed in Section III to the evolution of black hole spacetimes in the presence of matter fields, specifically focusing on the Reissner-Nordström (RN) black hole and a black hole that undergoes spontaneous scalarization within the Einstein-Maxwell-scalar (EMS) system [7, 39, 40]. Our numerical results strongly suggest that the CCZ3 formulation is the most robust and accurate for simulating long-term black hole evolution in the presence of matter fields.

A. Numerical evolution of matter fields

In the EMS system, a scalar field Φ (here assumed real for simplicity) is minimally coupled to gravity and non-minimally coupled to the electromagnetic field A_μ ,

$$S = \frac{1}{16\pi} \int d^4x \sqrt{-g} [R - 2\partial_\mu \Phi \partial^\mu \Phi - f(\Phi) F^{\mu\nu} F_{\mu\nu}], \quad (29)$$

where $F_{\mu\nu} = \partial_\mu A_\nu - \partial_\nu A_\mu$. The coupling function is chosen as $f(\Phi) = e^{\alpha_0 \Phi^2}$, a choice that ensures the existence of tachyonic-type instabilities in the vicinity of a RN black hole, provided the coupling constant α_0 is large enough [39]. Varying the action (29) with respect to the scalar and electromagnetic fields yields their equations of motion,

$$\square \Phi = \frac{1}{4} \dot{f}(\Phi) F^2, \quad (30)$$

$$\nabla_\mu F^{\mu\nu} = -\partial_\mu f(\Phi) F^{\mu\nu}, \quad (31)$$

where $\dot{f}(\Phi) = df(\Phi)/d\Phi$. The corresponding stress-energy tensor sourcing the Einstein equation (1) is given by

$$T_{\mu\nu} = \frac{1}{8\pi} \left[2\partial_\mu \Phi \partial_\nu \Phi - g_{\mu\nu} \partial_\rho \Phi \partial^\rho \Phi + f(\Phi) \left(2F_{\mu\rho} F_\nu{}^\rho - \frac{1}{2} g_{\mu\nu} F^2 \right) \right]. \quad (32)$$

The electromagnetic field also obeys a constraint equation given by the Gauss law: $\nabla_{[\rho} F_{\mu\nu]} = 0$. Similar to the CCZ4 approach to the Einstein equations, one can introduce quantities measuring the violation of the constraints, respectively Ψ_E for the electric field and Ψ_B for the magnetic field, by extending the electromagnetic field equations as [41]

$$\begin{aligned} \nabla^\mu (F_{\mu\nu} + g_{\mu\nu} \Psi_E) &= -\partial_\mu f(\Phi) F^{\mu\nu} + \kappa_E n_\nu \Psi_E, \\ \nabla^\mu (*F_{\mu\nu} + g_{\mu\nu} \Psi_B) &= \kappa_B n_\nu \Psi_B, \end{aligned} \quad (33)$$

where $*F_{\mu\nu}$ is the Hodge dual of $F_{\mu\nu}$, and κ_E and κ_B are damping factors aimed at reducing the amount of constraint violations.

Analogously to the projections defined in Eq. (4), we decompose the Maxwell field into electric and magnetic fields via

$$E_i = \gamma_i^\mu n^\nu F_{\mu\nu}, \quad B_i = \gamma_i^\mu n^\nu (*F_{\mu\nu}). \quad (34)$$

In relation to the scalar field, we also introduce the variable $\Pi = n^\mu \nabla_\mu \Phi$, which acts as the

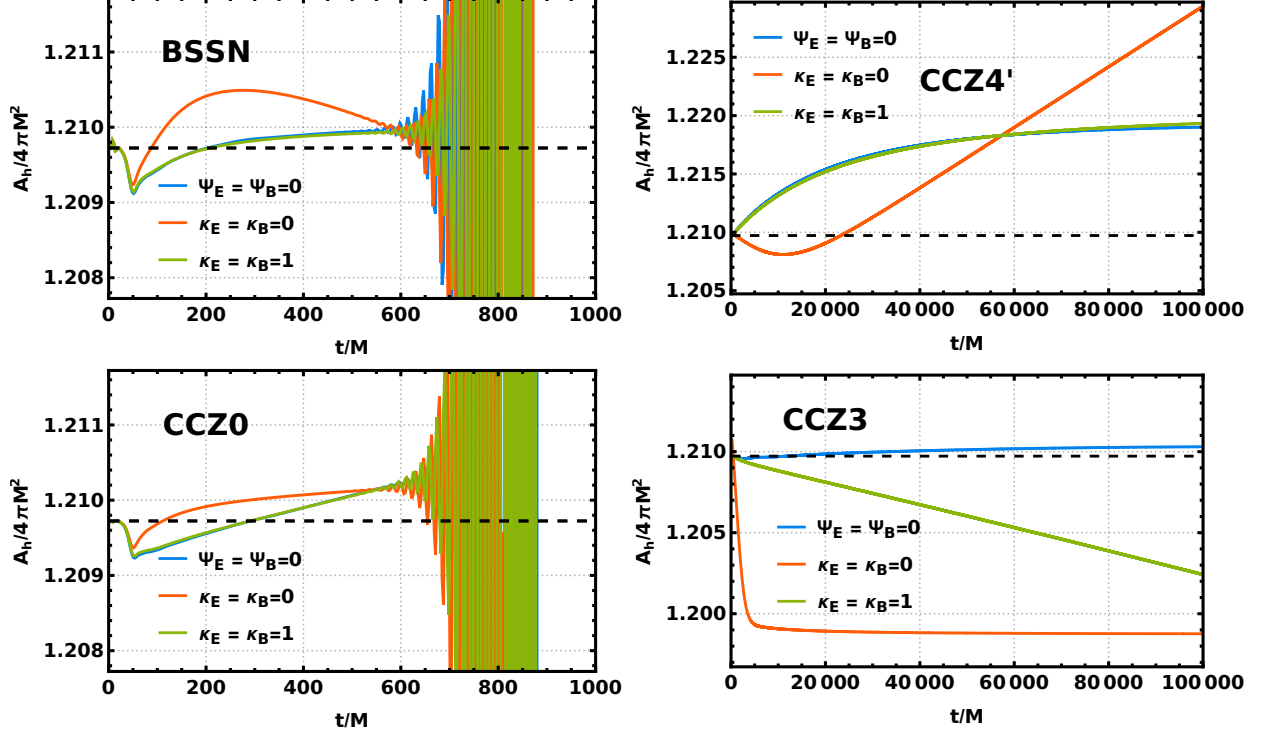


FIG. 4. Evolution of a RN black hole, as measured by the area of the apparent horizon, A_h , with $Q/M = 0.995$ and using various numerical schemes. The simulations demonstrate that the BSSN (upper-left panel) and CCZ0 (lower-left) formulations exhibit numerical instabilities at late times, while the CCZ4' (upper-right) and CCZ3 (lower-right) formulations propagate the constraint violations in a stable manner, maintaining accuracy without late-time divergences.

momentum of the field. The collected evolution equations for the matter fields are then given by

$$\begin{aligned}
\partial_{\perp}\Phi &= \alpha\Pi, \\
\partial_{\perp}\Pi &= D^i(\alpha D_i\Phi) + \alpha\Pi K - \frac{\alpha}{4}\dot{f}(\Phi)F^2, \\
\partial_{\perp}E^i &= \alpha KE^i - \alpha D^i\Psi_E + \epsilon^{ijk}D_j(\alpha B_k) + \alpha\frac{\dot{f}(\Phi)}{f(\Phi)}\left(\epsilon^{ijk}\partial_j\Phi B_k - E^i\Pi\right), \\
\partial_{\perp}\Psi_E &= -\alpha\left(\frac{\dot{f}}{f}D_i\phi E^i + D_iE^i + \kappa_E\Psi_E\right), \\
\partial_{\perp}B^j &= -\epsilon^{jkl}D_k(\alpha E_l) + \alpha(KB^j + D^j\Psi_B), \\
\partial_{\perp}\Psi_B &= \alpha(D_iB^i - \kappa_B\Psi_B).
\end{aligned} \tag{35}$$

B. RN black hole

Focusing first on the electric RN black hole spacetime, the initial data is given by [42]

$$e^{2\phi} = \left(1 + \frac{M}{2r}\right)^2 - \frac{Q^2}{4r^2}, \quad E^r = e^{-6\phi} \frac{Q}{r^2}, \quad B^i = 0, \quad \Phi = 0. \quad (36)$$

In Fig. 4 we present the results of several simulations of this spacetime, considering a large charge-to-mass ratio ($Q/M = 0.995$) in order to appreciate the differences relative to the vacuum case studied in Section III. The four panels in the figure correspond to the different numerical schemes: BSSN (upper-left panel), CCZ4' (upper-right), CCZ0 (lower-left) and CCZ3 (lower-right). Similarly to the simulation of a Schwarzschild black hole, the BSSN and CCZ0 formulations fail to maintain a stable numerical evolution at late times, exhibiting oscillating divergences. In contrast, the CCZ4' and CCZ3 formulations successfully simulate the evolution without encountering late-time instabilities, once again highlighting the virtue of the propagation of the momentum constraint Z_i in long-term simulations.

It is noteworthy that the propagation of constraint violations in the electromagnetic system does not lead to significant improvement in numerical stability. In particular, the CCZ3 formulation is observed to yield the most accurate results in the case where the electromagnetic constraints are defined as non-propagating, i.e. $\Psi_E = \Psi_B = 0$. This appears to apply in general, as suggested by similar findings in the hairy black hole model studied in the next subsection.

C. Spontaneous scalarization

We next simulate the evolution of the spontaneous scalarization mechanism of a charged black hole in the EMS model. The simulations start with a RN black hole background with the initial data of Eq. (36), along with a small initial perturbation of the scalar field corresponding to a spherical Gaussian wave-packet: $\delta\Phi = pe^{-\frac{r^2}{M^2}}$, with $p = 10^{-4}$. The coupling constant is set to $\alpha_0 = 1$, ensuring the scalarization rate is slow enough to call for robust long-term numerics. Fig. 5 displays the numerical evolution in the time domain of the system, in which the initial RN black hole evolves into a scalarized state with scalar hair. The numerical schemes are the same as in Fig. 4. Similarly to the vacuum and electro-vacuum cases, our results show that the BSSN and CCZ0 formulations do not provide robust results in the long term, failing in this case to fully capture the formation of the scalarized black hole, with the evolution diverging in a comparatively short time. In contrast, both the CCZ4' and CCZ3 formulations successfully establish stable long-term evolutions for the spontaneous scalarization process triggered by weak physical instabilities.

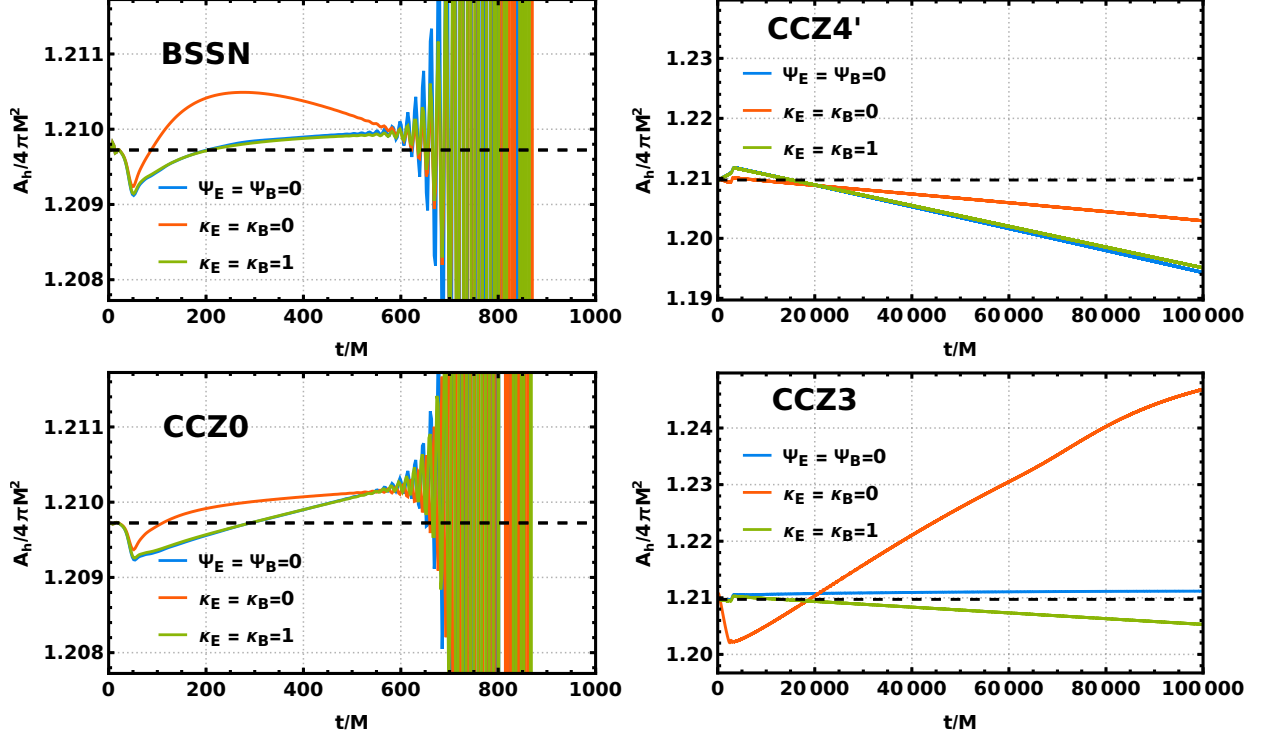


FIG. 5. The area of the apparent horizon, A_h , during the evolution of spontaneous scalarization in the EMS model with coupling constant $\alpha_0 = 1$. The evolution starts from the RN black hole with $Q/M = 0.995$ and an initial perturbation of the scalar field given by a Gaussian wave-packet (see the main text). The results indicate that only the CCZ4' (upper-right panel) and CCZ3 (lower-right) formulations yield stable long-term evolution and correctly simulate the formation of a scalarized black hole, whereas the BSSN (upper-left) and CCZ0 (lower-left) schemes fail to accurately do so.

Finally, we study the comparison of the two new proposed schemes, CCZ4' and CCZ3, and considering different choices for the numerical formulation of the electromagnetic field constraints. To this end, we introduce the quantity

$$\Delta A_h(t) = A_h^{\delta\Phi(p=10^{-4})}(t) - A_h^{\delta\Phi(p=0)}(t) + A_h^{\delta\Phi(p=0)}(0), \quad (37)$$

which effectively subtracts the background noise $A_h^{\delta\Phi(p=0)}(t)$, as a way to better track the area of the apparent horizon during the scalarization process. Additionally, we compute the scalar field value Φ_h at the location of the apparent horizon. In Fig. 6 we show the results of simulations using the two formulations. The CCZ4' scheme does not succeed to accurately simulate the evolution, at least insofar as the apparent horizon is concerned, which is seen not to converge (upper-left panel). On the other hand, the CCZ3 scheme is able to maintain numerical stability and yield convergent results, although we also learn that additional care is needed in the presence of constraints in the matter sector. In the case of the EMS system considered here, we see that different schemes for the

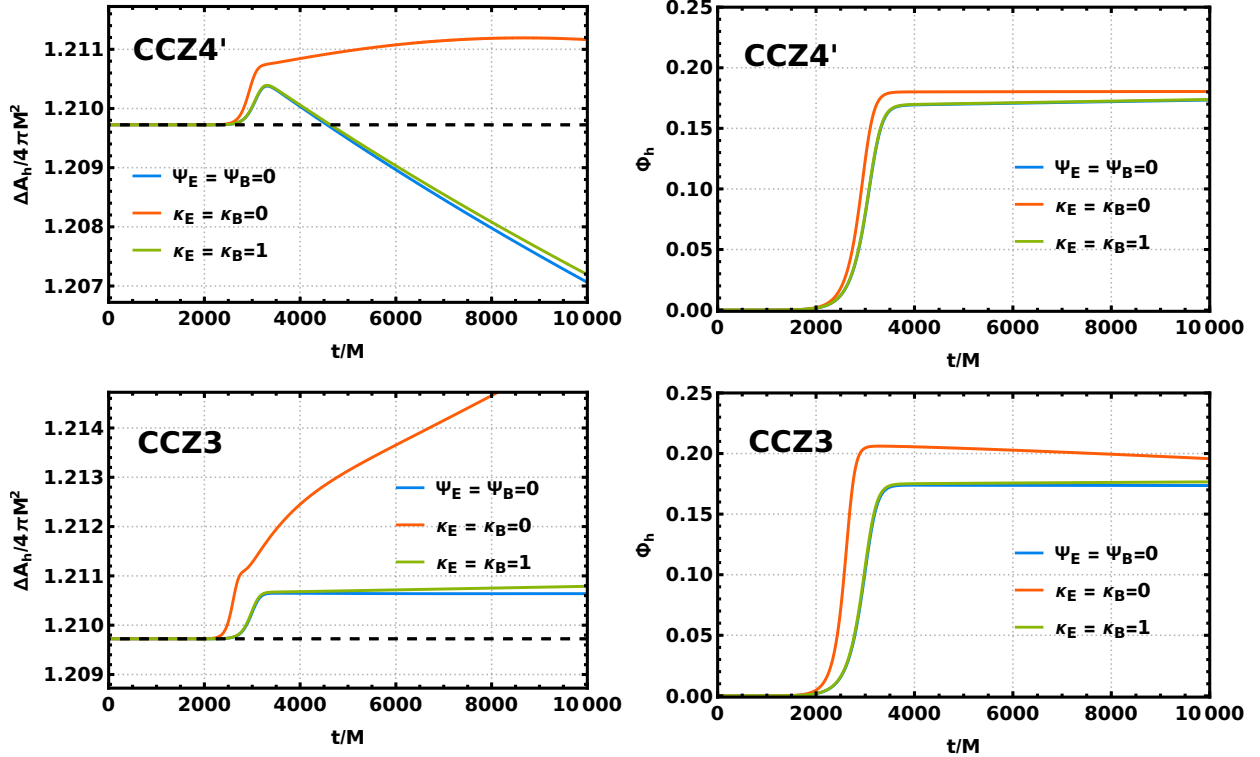


FIG. 6. The evolution of the subtracted apparent horizon area ΔA_h (left panels), cf. Eq. (37), and the horizon value of the scalar field Φ_h (right panels) for the spontaneous scalarization process, using the CCZ4' (upper panels) and CCZ3 (lower panels) formulations. The CCZ3 scheme is seen to exhibit the most accurate and robust results for the apparent horizon growth during the scalarization process, cf. in particular the blue line in the lower-left panel.

evolution of the Gauss constraints lead to different outcomes, with the choice that results in highest accuracy and stability being the setting with non-propagating constraints, i.e. $\Psi_E = \Psi_B = 0$ (cf. the blue curves in the lower panels of Fig. 6).

V. CONCLUSIONS

Our aim in this paper was to investigate the numerical stability of long-term black hole simulations within numerical relativity. We have identified a potential “late-time instability” in the evolution of static black holes, present already in the simplest context of the Schwarzschild spacetime, and which could not be resolved through various numerical manipulations. Drawing inspiration from the CCZ4 formulation, which is designed to propagate constraint violations as extra equations in order to enhance numerical stability, we have proposed several modified schemes aimed at mitigating this instability in black hole evolution.

Our numerical experiments with the evolution of a Schwarzschild black hole demonstrated that propagating the momentum constraint violation Z_i without introducing a damping effect successfully alleviates late-time numerical instabilities. Based on this observation, we introduced two modified versions of the CCZ4 formulation, referred to here as CCZ4' and CCZ3, both of which enable stable long-term evolution, reaching times of order $10^5 M$ in our simulations.

The advantage of the CCZ4 formulation over the BSSN approach is the implementation of constraint violations as propagating equations. Critical to the success of this method is the inclusion of appropriate damping factors. However, it has been appreciated that excessive damping may induce non-linear numerical instabilities, cf. Fig. 2 and Refs. [27, 30]. This observation underscores the need for a comprehensive assessment of different schemes in the implementation of damping factors in numerical relativity, which is precisely what we have endeavored to do in this paper.

We have found that this type of instabilities can be avoided provided that the damping effect on the momentum constraint violation, Z_i , is turned off, even with substantial damping applied to the Hamiltonian constraint violation Θ (cf. the upper-right panel of Fig. 2 where $\kappa_\Theta = 1$ and $\kappa_\Gamma = 0$). As a result, both the CCZ4' and CCZ3 formulations were shown to significantly enhance the numerical stability of black hole evolution over long time scales. The importance of the momentum constraint versus the Hamiltonian constraint, at least insofar as the long-term evolution of black holes is concerned, is further made clear by the drawbacks of the CCZ0 scheme, which we introduced specifically for the purpose of comparison.

To further test our proposed formulations, we also studied their application to black hole spacetimes with matter fields, concretely the EMS model described in Section IV. In these cases, we observed that the CCZ3 scheme is superior to the CCZ4', while also emphasizing that additional care is required in the presence of constraints in the matter sector of the theory. At least for the system we considered here, turning off the evolution of the matter constraints appears to be the appropriate choice in the context of physical instabilities with slow growth rates. It would be interesting to further test this numerical scheme in other set-ups with weak instabilities, such as rotating black holes undergoing superradiance.

ACKNOWLEDGMENTS

We are grateful to Yiqian Chen and Shenkai Qiao for useful discussions and valuable comments. SGS, GG and XW are supported by the NSFC (Grant Nos. 12250410250 and 12347133). PW is

supported in part by the NSFC (Grant Nos. 12105191, 12275183, 12275184 and 11875196).

-
- [1] B.P. Abbott et al. Observation of Gravitational Waves from a Binary Black Hole Merger. *Phys. Rev. Lett.*, 116(6):061102, 2016. [arXiv:1602.03837](#), [doi:10.1103/PhysRevLett.116.061102](#).
- [2] Kazunori Akiyama et al. First M87 Event Horizon Telescope Results. I. The Shadow of the Supermassive Black Hole. *Astrophys. J. Lett.*, 875:L1, 2019. [arXiv:1906.11238](#), [doi:10.3847/2041-8213/ab0ec7](#).
- [3] Kazunori Akiyama et al. First Sagittarius A* Event Horizon Telescope Results. I. The Shadow of the Supermassive Black Hole in the Center of the Milky Way. *Astrophys. J. Lett.*, 930(2):L12, 2022. [arXiv:2311.08680](#), [doi:10.3847/2041-8213/ac6674](#).
- [4] Manuela Campanelli, C. O. Lousto, P. Marronetti, and Y. Zlochower. Accurate evolutions of orbiting black-hole binaries without excision. *Phys. Rev. Lett.*, 96:111101, 2006. [arXiv:gr-qc/0511048](#), [doi:10.1103/PhysRevLett.96.111101](#).
- [5] Frans Pretorius. Evolution of binary black hole spacetimes. *Phys. Rev. Lett.*, 95:121101, 2005. [arXiv:gr-qc/0507014](#), [doi:10.1103/PhysRevLett.95.121101](#).
- [6] John G. Baker, Joan Centrella, Dae-Il Choi, Michael Koppitz, and James van Meter. Gravitational wave extraction from an inspiraling configuration of merging black holes. *Phys. Rev. Lett.*, 96:111102, 2006. [arXiv:gr-qc/0511103](#), [doi:10.1103/PhysRevLett.96.111102](#).
- [7] Guangzhou Guo, Peng Wang, and Yupeng Zhang. Nonlinear Stability of Black Holes with a Stable Light Ring. 3 2024. [arXiv:2403.02089](#).
- [8] T. Damour, N. Deruelle, and R. Ruffini. On Quantum Resonances in Stationary Geometries. *Lett. Nuovo Cim.*, 15:257–262, 1976. [doi:10.1007/BF02725534](#).
- [9] Asimina Arvanitaki, Savvas Dimopoulos, Sergei Dubovsky, Nemanja Kaloper, and John March-Russell. String Axiverse. *Phys. Rev. D*, 81:123530, 2010. [arXiv:0905.4720](#), [doi:10.1103/PhysRevD.81.123530](#).
- [10] Steven L. Detweiler. KLEIN-GORDON EQUATION AND ROTATING BLACK HOLES. *Phys. Rev. D*, 22:2323–2326, 1980. [doi:10.1103/PhysRevD.22.2323](#).
- [11] Vitor Cardoso, Oscar J. C. Dias, Jose P. S. Lemos, and Shijun Yoshida. The Black hole bomb and superradiant instabilities. *Phys. Rev. D*, 70:044039, 2004. [Erratum: *Phys.Rev.D* 70, 049903 (2004)]. [arXiv:hep-th/0404096](#), [doi:10.1103/PhysRevD.70.049903](#).
- [12] Sam R. Dolan. Superradiant instabilities of rotating black holes in the time domain. *Phys. Rev. D*, 87(12):124026, 2013. [arXiv:1212.1477](#), [doi:10.1103/PhysRevD.87.124026](#).
- [13] Nicolas Sanchis-Gual, Juan Carlos Degollado, Pedro J. Montero, José A. Font, and Carlos Herdeiro. Explosion and Final State of an Unstable Reissner-Nordström Black Hole. *Phys. Rev. Lett.*, 116(14):141101, 2016. [arXiv:1512.05358](#), [doi:10.1103/PhysRevLett.116.141101](#).
- [14] William E. East and Frans Pretorius. Superradiant Instability and Backreaction of Massive Vector

- Fields around Kerr Black Holes. *Phys. Rev. Lett.*, 119(4):041101, 2017. [arXiv:1704.04791](#), [doi:10.1103/PhysRevLett.119.041101](#).
- [15] Vitor Cardoso, Luís C. B. Crispino, Caio F. B. Macedo, Hirotada Okawa, and Paolo Pani. Light rings as observational evidence for event horizons: long-lived modes, ergoregions and nonlinear instabilities of ultracompact objects. *Phys. Rev. D*, 90(4):044069, 2014. [arXiv:1406.5510](#), [doi:10.1103/PhysRevD.90.044069](#).
- [16] Pedro V. P. Cunha, Carlos Herdeiro, Eugen Radu, and Nicolas Sanchis-Gual. Exotic Compact Objects and the Fate of the Light-Ring Instability. *Phys. Rev. Lett.*, 130(6):061401, 2023. [arXiv:2207.13713](#), [doi:10.1103/PhysRevLett.130.061401](#).
- [17] Masaru Shibata and Takashi Nakamura. Evolution of three-dimensional gravitational waves: Harmonic slicing case. *Phys. Rev. D*, 52:5428–5444, 1995. [doi:10.1103/PhysRevD.52.5428](#).
- [18] Thomas W. Baumgarte and Stuart L. Shapiro. On the numerical integration of Einstein’s field equations. *Phys. Rev. D*, 59:024007, 1998. [arXiv:gr-qc/9810065](#), [doi:10.1103/PhysRevD.59.024007](#).
- [19] J. David Brown. Covariant formulations of BSSN and the standard gauge. *Phys. Rev. D*, 79:104029, 2009. [arXiv:0902.3652](#), [doi:10.1103/PhysRevD.79.104029](#).
- [20] Ian Ruchlin, Zachariah B. Etienne, and Thomas W. Baumgarte. SENR/NRPy+: Numerical Relativity in Singular Curvilinear Coordinate Systems. *Phys. Rev. D*, 97(6):064036, 2018. [arXiv:1712.07658](#), [doi:10.1103/PhysRevD.97.064036](#).
- [21] Thomas W. Baumgarte and Stuart L. Shapiro. Relativistic radiation hydrodynamics in a reference-metric formulation. *Phys. Rev. D*, 102(10):104001, 2020. [arXiv:2009.08990](#), [doi:10.1103/PhysRevD.102.104001](#).
- [22] Ryosuke Urakawa, Takuya Tsuchiya, and Gen Yoneda. On the stability of covariant BSSN formulation. *Class. Quant. Grav.*, 39(16):165002, 2022. [arXiv:2206.13944](#), [doi:10.1088/1361-6382/ac7e16](#).
- [23] Daniela Alic, Carles Bona-Casas, Carles Bona, Luciano Rezzolla, and Carlos Palenzuela. Conformal and covariant formulation of the Z4 system with constraint-violation damping. *Phys. Rev. D*, 85:064040, 2012. [arXiv:1106.2254](#), [doi:10.1103/PhysRevD.85.064040](#).
- [24] Milton Ruiz, David Hilditch, and Sebastiano Bernuzzi. Constraint preserving boundary conditions for the Z4c formulation of general relativity. *Phys. Rev. D*, 83:024025, 2011. [arXiv:1010.0523](#), [doi:10.1103/PhysRevD.83.024025](#).
- [25] David Hilditch, Sebastiano Bernuzzi, Marcus Thierfelder, Zhoujian Cao, Wolfgang Tichy, and Bernd Bruegmann. Compact binary evolutions with the Z4c formulation. *Phys. Rev. D*, 88:084057, 2013. [arXiv:1212.2901](#), [doi:10.1103/PhysRevD.88.084057](#).
- [26] Sebastiano Bernuzzi and David Hilditch. Constraint violation in free evolution schemes: Comparing BSSNOK with a conformal decomposition of Z4. *Phys. Rev. D*, 81:084003, 2010. [arXiv:0912.2920](#), [doi:10.1103/PhysRevD.81.084003](#).
- [27] Nicolas Sanchis-Gual, Pedro J. Montero, Jose A. Font, Ewald Müller, and Thomas W. Baumgarte. Fully covariant and conformal formulation of the Z4 system in a reference-metric approach: comparison with

- the BSSN formulation in spherical symmetry. *Phys. Rev. D*, 89(10):104033, 2014. [arXiv:1403.3653](#), [doi:10.1103/PhysRevD.89.104033](#).
- [28] Vassilios Mewes, Yosef Zlochower, Manuela Campanelli, Thomas W. Baumgarte, Zachariah B. Etienne, Federico G. Lopez Armengol, and Federico Cipolletta. Numerical relativity in spherical coordinates: A new dynamical spacetime and general relativistic MHD evolution framework for the Einstein Toolkit. *Phys. Rev. D*, 101(10):104007, 2020. [arXiv:2002.06225](#), [doi:10.1103/PhysRevD.101.104007](#).
- [29] Gray D. Reid and Matthew W. Choptuik. Reference metric approach to the Z4 system. *Phys. Rev. D*, 108(12):124070, 2023. [arXiv:2309.05094](#), [doi:10.1103/PhysRevD.108.124070](#).
- [30] Daniela Alic, Wolfgang Kastaun, and Luciano Rezzolla. Constraint damping of the conformal and co-variant formulation of the Z4 system in simulations of binary neutron stars. *Phys. Rev. D*, 88(6):064049, 2013. [arXiv:1307.7391](#), [doi:10.1103/PhysRevD.88.064049](#).
- [31] Carles Bona, Joan Masso, Edward Seidel, and Joan Stela. A New formalism for numerical relativity. *Phys. Rev. Lett.*, 75:600–603, 1995. [arXiv:gr-qc/9412071](#), [doi:10.1103/PhysRevLett.75.600](#).
- [32] Miguel Alcubierre, Bernd Bruegmann, Peter Diener, Michael Koppitz, Denis Pollney, Edward Seidel, and Ryoji Takahashi. Gauge conditions for long term numerical black hole evolutions without excision. *Phys. Rev. D*, 67:084023, 2003. [arXiv:gr-qc/0206072](#), [doi:10.1103/PhysRevD.67.084023](#).
- [33] Erik Schnetter. Time Step Size Limitation Introduced by the BSSN Gamma Driver. *Class. Quant. Grav.*, 27:167001, 2010. [arXiv:1003.0859](#), [doi:10.1088/0264-9381/27/16/167001](#).
- [34] Zachariah B. Etienne and Ian Ruchlin et al. BlackHoles@Home, 2022, To find out more, visit <https://blackholesathome.net/>.
- [35] William H. Press, Saul A. Teukolsky, William T. Vetterling, and B. P. Flannery. *Numerical Recipes: The Art of Scientific Computing (Third Edition)*. Cambridge University Press, 2007.
- [36] J. David Brown. Probing the puncture for black hole simulations. *Phys. Rev. D*, 80:084042, 2009. [arXiv:0908.3814](#), [doi:10.1103/PhysRevD.80.084042](#).
- [37] Zachariah B. Etienne. Improved Moving-Puncture Techniques for Compact Binary Simulations. 4 2024. [arXiv:2404.01137](#).
- [38] Carsten Gundlach, Jose M. Martin-Garcia, Gioel Calabrese, and Ian Hinder. Constraint damping in the Z4 formulation and harmonic gauge. *Class. Quant. Grav.*, 22:3767–3774, 2005. [arXiv:gr-qc/0504114](#), [doi:10.1088/0264-9381/22/17/025](#).
- [39] Carlos A.R. Herdeiro, Eugen Radu, Nicolas Sanchis-Gual, and José A. Font. Spontaneous Scalarization of Charged Black Holes. *Phys. Rev. Lett.*, 121(10):101102, 2018. [arXiv:1806.05190](#), [doi:10.1103/PhysRevLett.121.101102](#).
- [40] Sebastian Garcia-Saenz, Guangzhou Guo, Peng Wang, and Xinmiao Wang. Black hole accretion of scalar clouds with spontaneous symmetry breaking. *Phys. Rev. D*, 110(12):124045, 2024. [arXiv:2409.13184](#), [doi:10.1103/PhysRevD.110.124045](#).
- [41] Eric W. Hirschmann, Luis Lehner, Steven L. Liebling, and Carlos Palenzuela. Black Hole Dynamics in Einstein-Maxwell-Dilaton Theory. *Phys. Rev. D*, 97(6):064032, 2018. [arXiv:1706.09875](#), [doi:](#)

[10.1103/PhysRevD.97.064032](https://doi.org/10.1103/PhysRevD.97.064032).

- [42] Miguel Alcubierre, Juan Carlos Degollado, and Marcelo Salgado. The Einstein-Maxwell system in 3+1 form and initial data for multiple charged black holes. *Phys. Rev. D*, 80:104022, 2009. [arXiv:0907.1151](https://arxiv.org/abs/0907.1151), [doi:10.1103/PhysRevD.80.104022](https://doi.org/10.1103/PhysRevD.80.104022).